Spectrum of Feshbach Resonances in NaLi + Na Collisions

Juliana J. Park,[1,*] Hyungmok Son,[1,2] Yu-Kun Lu,[1] Tijs Karman,[3] Marcin Gronowski,[4] Michał Tomza,[4] Alan O. Jamison,[5] and Wolfgang Ketterle[1]

[1]*Research Laboratory of Electronics, MIT-Harvard Center for Ultracold Atoms, Department of Physics, Massachusetts Institute of Technology, Cambridge, Massachusetts 02139, USA*
[2]*Department of Physics, Harvard University, Cambridge, Massachusetts 02138, USA*
[3]*Institute for Molecules and Materials, Radboud University, Heijendaalseweg 135, 6525 AJ Nijmegen, The Netherlands*
[4]*Faculty of Physics, University of Warsaw, Pasteura 5, 02-093 Warsaw, Poland*
[5]*Institute for Quantum Computing and Department of Physics and Astronomy, University of Waterloo, Waterloo, Ontario N2L 3G1, Canada*

(Received 1 March 2023; accepted 8 June 2023; published 14 August 2023)

Collisional resonances of molecules can offer a deeper understanding of interaction potentials and collision complexes, and allow control of chemical reactions. Here, we experimentally map out the spectrum of Feshbach resonances in collisions between ultracold triplet rovibrational ground-state NaLi molecules and Na atoms over a range of 1400 G. Preparation of the spin-stretched state puts the system initially into the nonreactive quartet potential. A total of 25 resonances are observed, in qualitative agreement with quantum-chemistry calculations using a coupled-channels approach. Although the theory cannot predict the positions of resonances, it can account for several experimental findings and provide unprecedented insight into the nature and couplings of ultracold, strongly interacting complexes. Previous work has addressed only weakly bound complexes. We show that the main coupling mechanism results from spin-rotation and spin-spin couplings in combination with the anisotropic atom-molecule interaction, and that the collisional complexes which support the resonances have a size of $30a_0$–$40a_0$. This study illustrates the potential of a combined experimental and theoretical approach.

DOI: 10.1103/PhysRevX.13.031018

Subject Areas: Atomic and Molecular Physics, Physical Chemistry, Quantum Physics

I. INTRODUCTION

Collisional resonances that are electromagnetically tunable have become an established tool for modifying interactions between ultracold atoms and are the key for many applications, from magnetic association of loosely bound molecules to quantum simulations [1,2]. For ultracold molecular systems, tunable collisional resonances can control chemical reactions [3] and also provide microscopic information about interaction potentials and collision complexes.

In the case of cold collisions between alkali-metal *atoms*, the number of resonant states remains typically small, and the resonances are usually tractable. However, in the case of cold collisions involving *molecules*, due to strong and anisotropic interactions, rovibrational excited states can also contribute to resonant states, and therefore resonances themselves may not be well separated and are difficult to identify. Because of the large density of states of molecular systems [4,5] it has been a challenge to perform rigorous scattering calculations, and different methods of approximations have become an active field [6,7]. Despite these efforts, due to the extreme sensitivity of the low-temperature observables to details of potential energy surfaces [8,9], there has been very little success in predicting Feshbach resonances in molecular collisions.

Rather than performing exact quantum calculations, one feasible alternative approach is the use of simple statistical short-range models while treating the physics of long-range scattering within multichannel quantum defect theory. This has been pursued for the description of molecular resonances [4,5,10,11]. However, the validity of statistical short-range models is controversial and, therefore, detailed experimental and further theoretical studies are needed.

Previously, only resonances supported by long-range states of collision complexes could be assigned to specific quantum states since the quantum numbers of the separated atoms and molecules are approximately preserved. Resonant states in collisions involving Feshbach molecules [12–15]

*jjpark@mit.edu

and in collisions between ^{40}K and ground-state ^{23}Na^{40}K$(X^1\Sigma^+)$ [16,17] were successfully analyzed in this way. Here we are addressing the challenge of more strongly interacting complexes by using, for the first time, a combined experimental and theoretical quantum-chemistry approach toward this goal. The agreement between experiment and theory validates approximations in the calculations, and the theoretical results can then be used to assign quantum numbers to resonances and to identify the microscopic mechanism of the resonant couplings. To keep the problem tractable, we focus on collisions between triplet rovibrational ground-state NaLi and Na, both prepared in the maximally spin-stretched state. Collisions of ^{23}Na^{6}Li$(a^3\Sigma^+)$ with Na are generally chemically reactive [^{23}Na^{6}Li$(a^3\Sigma^+)$ + Na → $Na_2(X^1\Sigma_g^+)$ + Li + heat]. However, the chemical reaction in the fully spin-polarized atom-molecule system is strongly suppressed due to the approximate conservation of the total spin [18,19], and we can regard NaLi + Na in the quartet potential as approximately chemically stable. The system is suitable for modeling molecular scattering resonances because of the relatively small density of states and number of electrons, and therefore more accurate quantum calculations are feasible compared to other heavier molecular systems. Although the observed resonances involve strongly bound complexes, we can make complete assignments of spin states and total mechanical angular momentum and identify the relevant coupling terms.

In previous work, we have analyzed the line shape of one very strong resonance in collisions between ^{23}Na and ^{23}Na^{6}Li$(a^3\Sigma^+)$ [18]. Here we report a study of collisions in both spin-stretched states over a magnetic field range of over 1400 G and report more than 20 new Feshbach resonances. This now allows us to draw conclusions about typical features of collisional complexes. The direct comparison with quantum chemistry calculations provides major new insight into the interaction potential and coupling mechanism of the strongly interacting collision complex.

II. EXPERIMENTAL PROTOCOL AND RESULTS

We prepare a mixture of triplet ground-state ^{23}Na^{6}Li$(a^3\Sigma^+)$ molecules and ^{23}Na atoms in the spin-polarized quartet

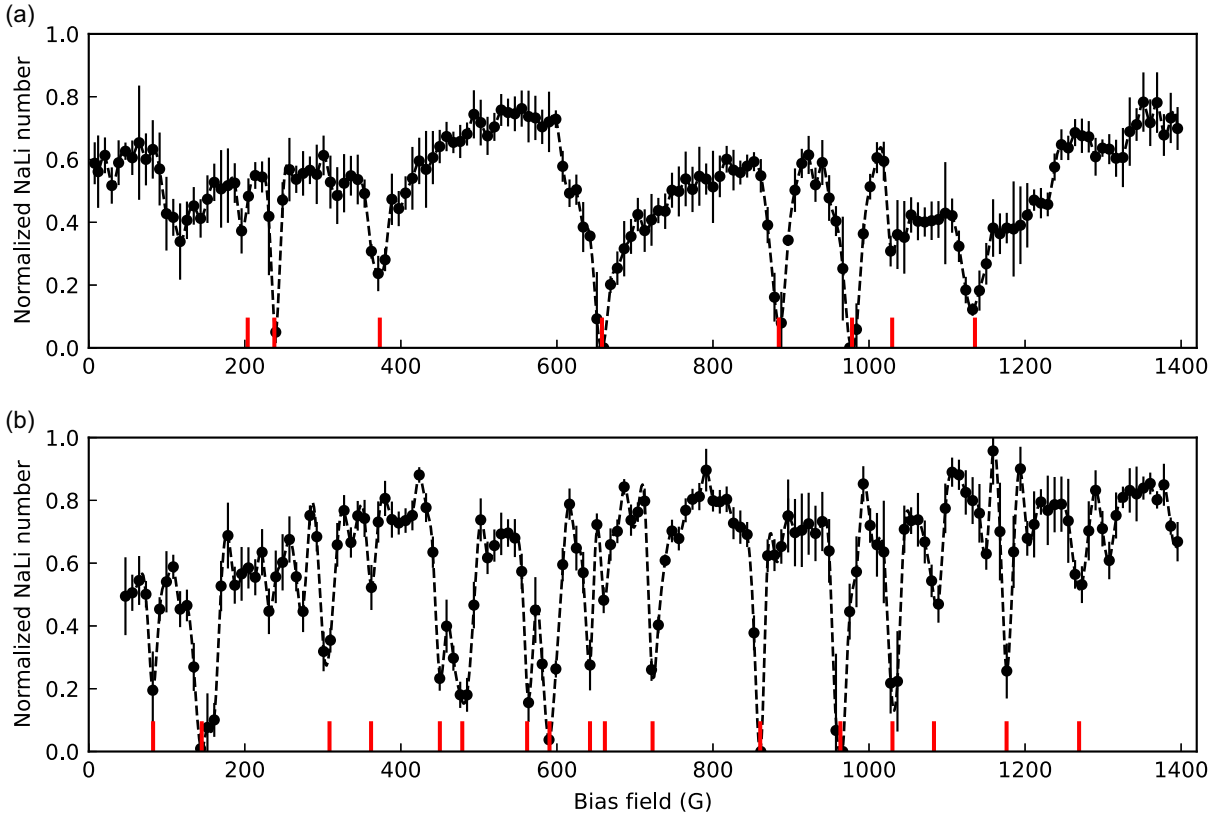

FIG. 1. Collisional loss spectrum of NaLi molecules with Na atoms as a function of magnetic field. Spectra are recorded for both the upper (a) and lower (b) stretched hyperfine states. Shown is the normalized number of NaLi molecules left after sweeping down the bias field by 13 G for 200 ms. The number of Na atoms in each pancake is around 115, and the initial number of NaLi molecules is about 35 at temperatures of $T_{Na} \approx T_{NaLi} \approx 1.6$ μK, corresponding to an overlap density of about 1.1×10^{11} cm^{-3}. A total of 25 resonances, indicated by red lines, are observed: 8 in the upper spin-polarized mixture and 17 in the lower spin-polarized mixture. Each data point represents 3–8 measurements. Error bars correspond to one standard deviation of the mean. Dashed lines are a guide to the eye, obtained by interpolating data with a piecewise cubic polynomial.

potential. There are two possible states: the "upper stretched state," where all nuclear and electron spins are aligned to the bias magnetic field direction ($|F, M_F\rangle_{\mathrm{NaLi}} + |F, M_F\rangle_{\mathrm{Na}} = |7/2, 7/2\rangle_{\mathrm{NaLi}} + |2, 2\rangle_{\mathrm{Na}}$), and the "lower stretched state," where all nuclear and electron spins are antialigned to the field direction ($|7/2, -7/2\rangle_{\mathrm{NaLi}} + |2, -2\rangle_{\mathrm{NaLi}}$). Here, F is the quantum number for the total spin (electron and nuclear) and M_F is the B-field projection of F. The molecule and atom mixture in the upper stretched state with typical numbers of $\sim 3 \times 10^4$ and $\sim 3 \times 10^5$, respectively, is produced at a temperature of $T_{\mathrm{Na}} \approx T_{\mathrm{NaLi}} \sim T = 1.55$ μK in a 1596 nm one-dimensional optical lattice following the method described in Refs. [18,20]. The lower stretched state is produced by coherent transfer from the sample in the upper stretched state using a magnetic field sweep in the presence of radio frequency waves [21]. For this process, the bias field is dropped from 745 G, where the upper stretched state is prepared, to a low field of around 8 G in 15 ms. After state preparation, the bias field is ramped to a target value in 15 ms. Collisional lifetimes of the atom-molecule mixtures are determined by holding the sample for a variable time at the target magnetic field.

The loss of NaLi molecules with Na atoms is measured as a function of the bias field for both spin-polarized states. First, we perform a coarse search by sweeping the bias field over a range of 12.6 G during 200 ms and recording the number of remaining molecules, normalized to the number without the field sweep. This procedure is repeated over a range from near zero to 1420 G in steps of 8.76 G, with the results shown in Fig. 1.

Near the loss features found in the coarse scan, finer scans are performed with sweep range and step size of around 1 G. We identify 8 resonances in the upper stretched state and 17 resonances in the lower stretched state indicated with red vertical lines in Fig. 1. Some structures visible in Fig. 1 which are not marked with red lines are not reproduced by the fine scans and could therefore not be distinguished from background loss. Using the data from the fine scans, each loss feature is fit to a Lorentzian with a slope accounting for background loss and nearby resonances [an example is shown in Fig. 2(a)]. For all resonances, the thus obtained peak positions and widths are listed in Table I. Strong losses lead to a broadened line shape. Therefore, for three resonances (labeled 4, 5, and 6 in the upper stretched state), we also determine the atom loss as a function of hold time and determine loss rates as a function of the bias field. These results are used for a more accurate determination of the resonance position and width, as shown in Fig. 2(b). We confirm that the width obtained from observed loss features can be broader than the width from the loss rate measurement. Figure 2 illustrates this for resonance 5 in the upper stretched state which is near 884 G. The width obtained from a Lorentzian fit to the loss feature is 17(1) G, whereas the loss rate measurements give a width of 10(2) G.

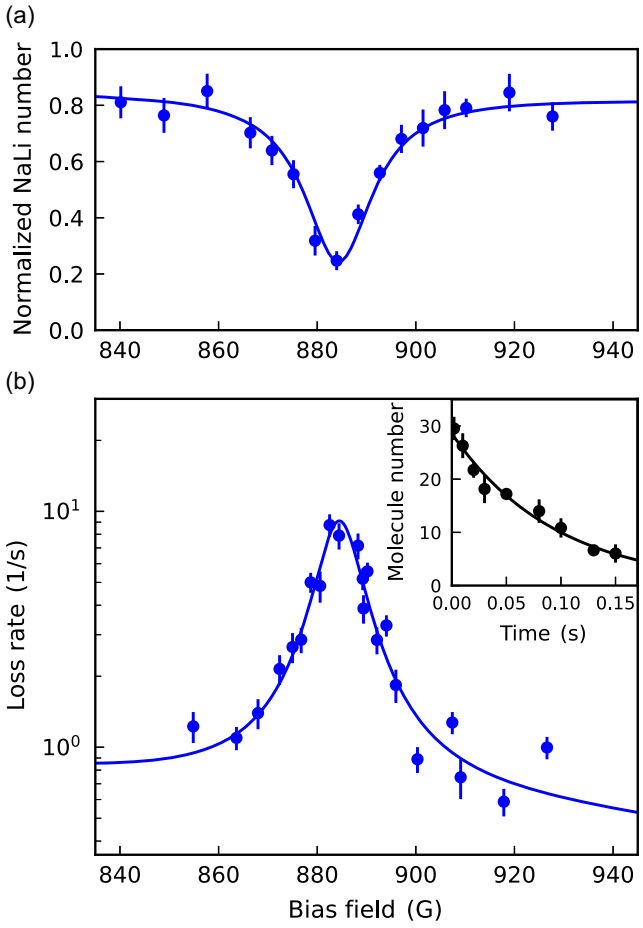

FIG. 2. Feshbach resonance near 884 G. This resonance is observed for NaLi + Na in the upper stretched state. (a) Normalized NaLi number as a function of bias field after a hold time of 100 ms. (b) Loss rate of NaLi molecules obtained from decay curves as shown in the inset at 884.3 G. Data values and error bars in (a) and inset of (b) represent the average and one standard deviation of the mean, estimated from statistical errors of 3–6 measurements, respectively. Error bars in the main plot of (b) represent one standard deviation of a fitted decay parameter. The blue lines are the fits to a Lorentzian function plus a background with a linear slope.

For all resonances, we determine peak loss rate constants β by recording decay curves as a function of the hold time near the center of the loss features. They are summarized in the last column of Table I. The determination of loss rate constants requires knowledge of the densities of sodium atoms overlapped with molecules. Instead of absolute calibration, we follow Ref. [18] and compare measured decay rates with the decay rate of the mixture in a nonstretched spin state which occurs at the universal rate [22]. This approach was validated in Ref. [18].

Away from resonances, the observed background loss rates are more than an order of magnitude smaller than the universal loss rate constant which for Na + NaLi s-wave collisions is 1.7×10^{-10} cm^3 s^{-1}. More specifically, at low

TABLE I. Observed Feshbach resonances. Resonance positions and widths are obtained by Lorentzian fits to loss features, except for resonances 4–6 for the incoming collision channel $|7/2,7/2\rangle_{\mathrm{NaLi}}+|2,2\rangle_{\mathrm{Na}}$. For these resonances, the position and width are determined by Lorentzian fits to the field-dependent loss rates [18].

Collision channel: $\lvert 7/2,7/2\rangle_{\mathrm{NaLi}}+\lvert 2,2\rangle_{\mathrm{Na}}$			
	B_0 (G)	ΔB (G)	β (cm^3 s^{-1})
1	203.7(2)	5.3(7)	$1.5(6)\times10^{-11}$
2	237.9(1)	6.3(4)	$7.1(1)\times10^{-11}$
3	372.0(7)	20(3)	$2.3(5)\times10^{-11}$
4	657.8(3)	5.2(8)	$1.0(1)\times10^{-10}$
5	884.3(3)	10(2)	$6(1)\times10^{-11}$
6	978.2(2)	4.9(3)	$7.4(5)\times10^{-10}$
7	1029.7(3)	10(2)	$1.5(3)\times10^{-11}$
8	1135.2(8)	15(3)	$3.0(5)\times10^{-11}$
Collision channel: $\lvert 7/2,-7/2\rangle_{\mathrm{NaLi}}+\lvert 2,-2\rangle_{\mathrm{Na}}$			
	B_0 (G)	ΔB (G)	β (cm^3 s^{-1})
1	82.5(1)	1.3(2)	$1.0(3)\times10^{-10}$
2	145(1)	18(4)	$5.3(9)\times10^{-11}$
3	309(1)	13(4)	$1.9(4)\times10^{-11}$
4	361.82(5)	1.0(2)	$4.5(8)\times10^{-11}$
5	449.8(2)	3.1(5)	$6(2)\times10^{-11}$
6	478(3)	35(13)	$3.4(6)\times10^{-11}$
7	561.8(2)	2.4(6)	$8(2)\times10^{-11}$
8	590.7(2)	9(1)	$8(2)\times10^{-11}$
9	642.3(5)	3(2)	$2.9(4)\times10^{-11}$
10	661.5(2)	3.9(9)	$2.4(5)\times10^{-11}$
11	722.5(1)	2.7(3)	$8(4)\times10^{-11}$
12	860.8(2)	2.1(6)	$2.4(6)\times10^{-10}$
13	963.3(2)	6(1)	$2(1)\times10^{-10}$
14	1030.1(2)	3.3(8)	$9(3)\times10^{-11}$
15	1083.3(3)	4(1)	$5(1)\times10^{-11}$
16	1176.3(3)	3.2(9)	$8(2)\times10^{-11}$
17	1269.2(1)	2.6(3)	$3.3(5)\times10^{-11}$

field near 0.5 G, the upper and lower stretched Na + NaLi loss rate constants are $7.5(2.2)\times10^{-12}$ and $6.7(2.0)\times10^{-12}$ cm^3 s^{-1}, respectively, and at high field (near 540 G), they are $4.5(1.4)\times10^{-12}$ and $3.5(1.0)\times10^{-12}$ cm^3 s^{-1}, respectively. Within the accuracy of measurement, the two stretched states have the same loss rate constants, with lower background loss rates at higher magnetic fields.

III. ANALYSIS

In this section, we summarize the experimental findings and draw some conclusions. First, we observe similar rates of background loss and Feshbach enhanced losses for both stretched states. This implies that Zeeman energies do not play a major role and that dipolar relaxation is not the dominant decay mechanism. Instead, the decay is probably dominated by shorter-range chemical reactions or inelastic loss, which are expected to be similar for both spin-stretched initial states. Regarding the number of resonances, we have observed more resonances for the lower stretched state. In the range up to 1400 G, we observed 8 resonances in the upper stretched state and 17 in the lower stretched state. Intuitively this observation can be rationalized that for the lower stretched state, the noninitial Zeeman states are closed channels that can support additional resonance states. Surprisingly, our quantum-chemistry calculations below show that the difference is instead caused by fast decay of some upper stretched state resonances that become too broad to be observed.

Next, we discuss the widths and spacings between resonances. The linewidths of the resonances range from about 1 G to about 30 G. If the linewidths are interpreted as due to the finite lifetime of the resonant state, this implies atom-molecule complexes with lifetimes in the range of 10 to 350 ns. Note that this interpretation cannot be applied to the strongest resonances including the resonance 6 in the upper stretched state near 978 G, in which the peak loss rate is close to the unitarity limit. In these cases, the resonances are associated with long-lived complexes. The broadening of the linewidths by the finite lifetime of the resonant state is small, and the resonance coupling strength determines the linewidth [18]. The average spacing between resonances is around 100 G. One possible interpretation of the spacing is rotational structure of the intermediate complex. The spacing between resonances of the order of 100 G corresponds to single spin-flip energy differences of 280 MHz. A rotational constant of this value corresponds to the moment of inertia of a complex with a size (i.e., atom-molecule separation) of around $30a_0$. Note that the rotationally excited states of the NaLi triplet molecules with $N=1$ are at 9.25 GHz and $N=2$ are at 27.75 GHz [23] corresponding to a double spin-flip energy at 1650 and 5000 G. In the accompanying paper, we show that this may lead to strong resonant features [24], but these occur far outside the magnetic field range studied here.

Finally, we can perform a statistical analysis of the distribution of nearest-neighbor resonance spacings. The observed distribution follows the Wigner-Dyson distribution [25,26], which is a feature of a chaotic system (see the Appendix). However, statistical conclusions from only 17 resonances are only tentative.

IV. COUPLED-CHANNELS CALCULATIONS

With the coupled-channels calculations we try to answer the following questions. (1) What is the mechanism of coupling between the initial scattering channel and the loss channels for the background loss? (2) What are the dominant interactions that are responsible for the resonances? (3) Why are there more observed resonances for the lower stretched state? (4) What quantum numbers describe the collisional complex? (5) What is the size of the collisional complex?

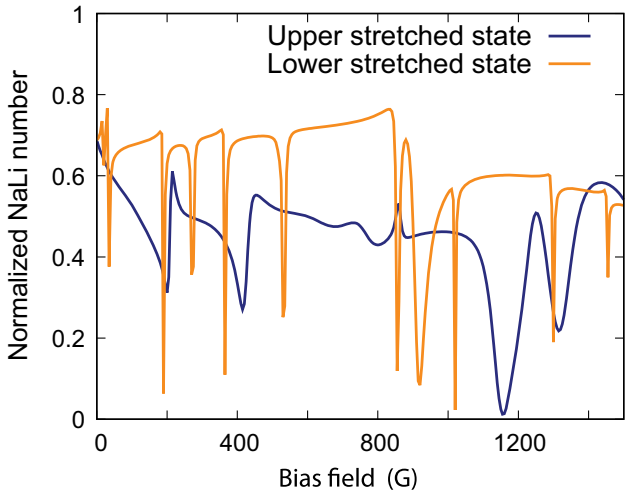

FIG. 3. Calculated spectrum of Feshbach resonances. Plotted are the calculated resonances for the upper and lower stretched states for $N_{\max} = 30$ and $\lambda = -0.02$. The comparison with Fig. 1 shows that most experimental features (except for resonance positions) are reproduced by the calculations. Shown is the normalized number of NaLi molecules left after 800 ms hold time, i.e., 4 times longer than in the experiment. This discrepancy is partially explained by the observation of higher elastic cross sections than expected [20], since we can show that the magnitudes of the elastic and inelastic cross sections are correlated [24].

The main result is shown in Fig. 3. A calculated spectrum reproduces most of the observed features (magnitude of loss rate, widths and number of resonances, more resonances for the lower stretched states), but cannot predict the observed resonance positions. This illustrates the power (and limitations) of state-of-the-art quantum-chemistry calculations.

These calculations are fully quantum mechanical coupled-channel calculations including the electronic interactions, the Zeeman interaction with the magnetic field, the magnetic dipole-dipole interaction, and the spin-rotation,

$$\hat{H}_{\text{spin-rotation}} = \gamma_s \hat{N} \cdot \hat{s}, \tag{1}$$

and spin-spin couplings,

$$\hat{H}_{\text{spin-spin}} = \lambda_s \sqrt{30}/3 [[\hat{s} \otimes \hat{s}]^{(2)} \otimes C^{(2)}(\hat{r}_{\text{NaLi}})]_0^{(0)}, \tag{2}$$

where the spin-spin coupling parameter $\lambda_s = 0.0189$ cm^{-1} and the spin-rotation coupling $\gamma_s = 0.005$ cm^{-1} are used [24]. Here, $[\hat{A} \otimes \hat{B}]_q^{(k)}$ indicates a tensor product, and $C^{(2)}(\hat{R})$ is a tensor of Racah-normalized spherical harmonics. The electronic interaction is partitioned into two-body interactions that are taken from experiment [27–29] and a nonadditive three-body interaction that is calculated with state-of-the-art coupled-cluster methods including single, double, and triple excitations with large Gaussian basis sets extrapolated to the complete basis set limit that are described in the accompanying paper [24]. The interaction-induced variation of spin-rotation and spin-spin couplings is neglected. We assume that the molecular bond length is fixed at the equilibrium position of the triplet potential, which does not describe the chemical reactions that form singlet NaLi or Na_2 molecules at the low-spin potential. In our coupled-channel calculations, we model these by imposing an absorbing boundary condition at $R = 4.5a_0$, which can be reached on the low-spin potential, but not on the high-spin potential, which is highly repulsive at these short distances. To reflect the error related to the rigid rotor approximation, we use a conservatively estimated uncertainty of the three-body interaction of ±5% [24]. In addition to this uncertainty, freezing the NaLi vibrational coordinate reduces the density of states of the collision complex by 50%, as we determine by quasiclassical calculations of the density of states with and without the rigid rotor approximation [24]. We thus expect that the rigid rotor approximation affects our conclusions only quantitatively, but not qualitatively.

For simplicity, we start by ignoring hyperfine and vibrational degrees of freedom. The scattering wave function is expanded in the basis of fully coupled-channel functions of the form

$$\begin{aligned} &|(NL)J(s_{\text{mol}}, s_{\text{atom}})S; \mathcal{J}\mathcal{M}\rangle \\ &\quad = \sum_{M_J, M_S} \langle JM_J SM_S | \mathcal{J}\mathcal{M}\rangle \\ &\qquad \times |(NL)JM_J\rangle |(s_{\text{mol}} s_{\text{atom}})SM_S\rangle, \end{aligned} \tag{3}$$

where $\langle JM_J SM_S | \mathcal{J}\mathcal{M}\rangle$ is a Clebsch-Gordan coefficient. The quantum number N represents the rotational angular momentum of the NaLi molecule, and L the angular momentum associated with the relative motion of the atom and molecule. N and L are Clebsch-Gordan coupled to a total mechanical angular momentum J with z-component M_J. Similarly, $s_{\text{mol}} = 0$ or 1 denotes the NaLi molecular electronic spin and $s_{\text{atom}} = 1/2$ is the atomic electronic spin, and S the total electronic spin with B-field projection M_S. In the coupled basis, J and S are subsequently coupled to a total angular momentum $\mathcal{J}$ and a magnetic field projection $\mathcal{M} = M_J + M_S$. $\mathcal{M}$ is strictly conserved, whereas, for a large enough magnetic field, M_S becomes a good quantum number and therefore $M_J = \mathcal{M} - M_S$ is also a good quantum number. Because of the large singlet-triplet splitting in the NaLi molecule, $s_{\text{mol}} = 0$ or 1 is also a good quantum number. For a separated atom and molecule, $m_{s_{\text{mol}}}$ and $m_{s_{\text{atom}}}$ would separately become good quantum numbers, but at chemically relevant distances the exchange splitting between the doublet and quartet interaction potentials is dominant, so that $S = 1/2$ and $3/2$ are good quantum numbers. Hence, we can effectively consider each $|SM_S\rangle$ state separately, with only perturbatively weak

couplings between them. For each of these spin channels, there are strong and anisotropic interactions that couple different N and L channels but conserve J and M_J. Since we ignore nuclear spin, the initial channel corresponds to s-wave collisions in the upper spin-stretched ground state $|(NL)JM_J\rangle|SM_S\rangle = |(00)00\rangle|3/23/2\rangle$ or the lower spin-stretched state $|(00)00\rangle|3/2,-3/2\rangle$. The full description of the Hamiltonian and matrix elements in the channel basis is given in the Appendix of the accompanying paper [24].

First, we consider the sensitivity of the scattering rates to the interaction potential shown in Fig. 4(a). Here, we scale by a factor $1+\lambda$ the nonadditive three-body part of the interaction potential, that is, the part that is computed *ab initio* and is uncertain up to a conservatively estimated 5%. By modifying the potential by only 0.1%, we find that the resonances start to shift so that realistically their positions are completely undetermined, and when the scaling reaches several percent we tune across magnetic field-independent resonances, indicating that the background scattering length is undetermined. Next, shown in Fig. 4(b), we again scale the three-body interaction but now only for the low-spin doublet potential, leaving the high-spin quartet potential unchanged. In this case, we find that several of the resonances are now completely independent of the scaling of the low-spin potential up to $\lambda = 0.1$. This implies that no stable resonance states are supported by the chemically reactive low-spin potential and that all the predicted (and observed) resonances originate in the quartet potential.

The analysis above indicates that the *ab initio* prediction of resonance positions is beyond the capability of state-of-the-art calculations. Although the coupled-channels calculations cannot predict the positions of the resonances, we can still use these calculations as a "numerical experiment" to investigate the nature of the resonance states, the coupling mechanisms, and the observed differences between the two spin-stretched states.

We perform coupled-channels scattering calculations with the interactions scaled by $1+\lambda$ and analyze the *typical* behavior observed for different λ between -0.1 and $+0.1$. Representative magnetic field scans can be seen in Fig. 5(a). With the truncation of the maximum rotational quantum number $N_{\max} = 30$, we observe a converged number of resonances of approximately 10 in the lower spin-stretched state and only around 5 in the upper spin-stretched state, respectively. This is in qualitative agreement with the experiment which observes 17 and 8 resonances, respectively. In the companion paper we show that based on the density of states we would expect to see approximately 10 resonances for either spin-stretched state [24]. We furthermore show that including molecular vibrations would increase the density of states by approximately 50%, which can partially explain the lower number of observed resonances compared to experiment. We show that including hyperfine interactions increases the density of resonances somewhat. With these effects in mind, one could claim almost quantitative agreement with experiment regarding the density of resonances.

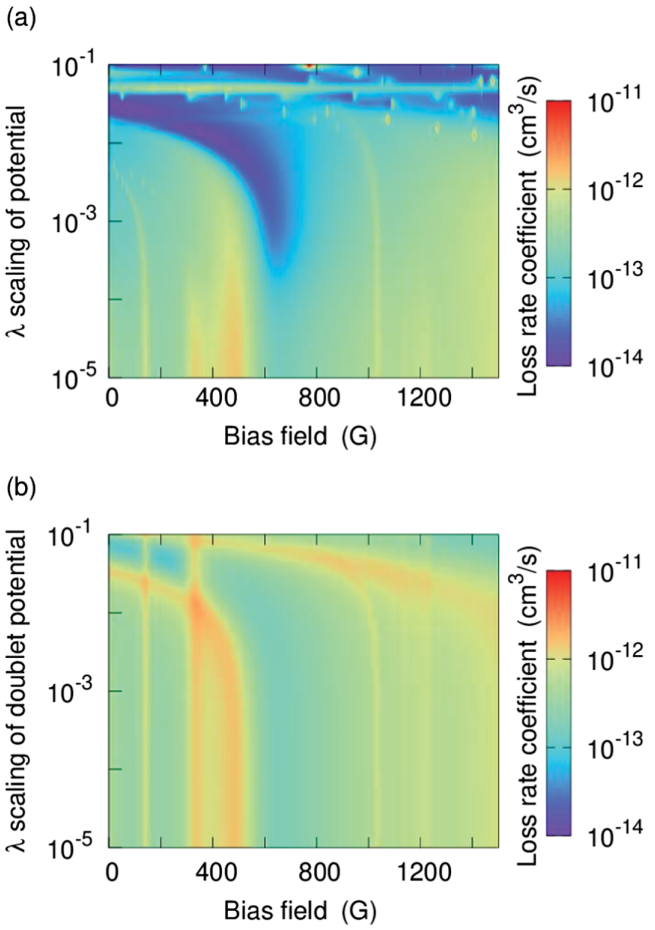

FIG. 4. Calculated loss rates as a function of magnetic field. Calculations are done with scaling of the spin-independent three-body interaction by a factor $1+\lambda$ for $N_{\max} = 6$. (a) Scaling of the three-body interaction for both the doublet and quartet state. The figure shows that scaling the three-body interactions within their uncertainty of at least several percent dramatically changes the loss rates: The positions of several Feshbach resonances change, and several B-independent resonances appear when the λ scaling creates a resonance in the initial spin-stretched potential, i.e., a bound state near zero energy. The conclusion is that the prediction of resonance positions and background loss requires knowledge of the interaction potentials to an accuracy better than can be achieved by *ab initio* calculations. (b) Scaling of the three-body interaction only for the doublet potential. In this case, the resonances follow vertical lines and are independent of the scaling up to $\lambda = 0.1$, implying that the resonances originate in the quartet potential.

One may expect that the lower spin-stretched state supports more magnetically tunable resonances because the noninitial Zeeman states correspond to closed channels—and hence can support Feshbach resonances—even in the rotational ground state, whereas closed channels for the upper spin-stretched state occur only for excited rotational

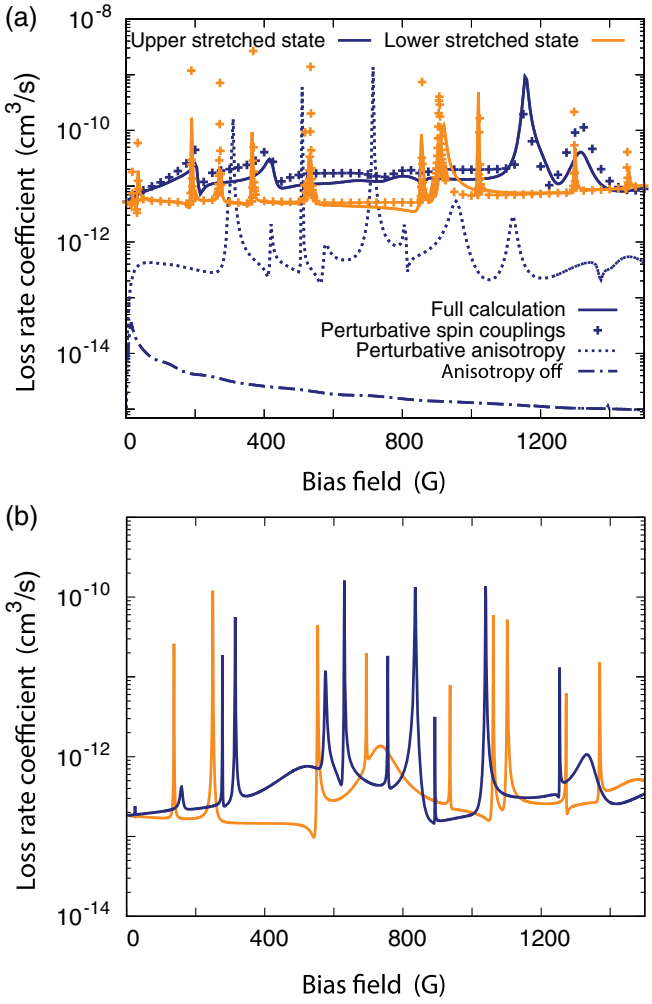

FIG. 5. Calculated spectrum of Feshbach resonances. (a) Results for the upper and lower spin-stretched states are shown in orange and blue solid lines (same data as in Fig. 3). The lower spin-stretched state typically shows around 10 resonances below 1500 G, whereas the upper spin-stretched state shows around half as many resonances. This qualitative difference between the two states is also observed experimentally. We investigate whether the anisotropy of the electronic interaction and the spin-spin and spin-rotation coupling act perturbatively, by scaling down these couplings by a factor of 2 and scaling the resulting cross section up by a factor 4. Agreement with the full calculation indicates the spin-spin and spin-rotation coupling act perturbatively, whereas the interaction anisotropy does not. The coupling mechanism however does involve the anisotropy, as turning this off entirely produces a much smaller cross section dominated by the magnetic dipole-dipole interaction (dash-dotted line). When both anisotropy and dipole-dipole are turned off, the calculated cross section is zero. (b) Removal of Zeeman states. The qualitative differences in the number of resonances for the upper and lower spin-stretched states disappear when we *exclude* from the calculation channels corresponding to Zeeman states in the rotational ground state, except for the initial Zeeman state.

states. We investigate this in our coupled-channels calculations by artificially excluding the noninitial Zeeman states in the rotational ground state; see Fig. 5(b). Somewhat surprisingly we find that *excluding* channels from the calculation does not reduce the number of resonances for the lower spin-stretched state, but rather increases the observed number of resonances for the upper spin-stretched state, where the excluded channels correspond to asymptotically open channels. In the presence of these open channels some of the resonances decay rapidly by spin-spin coupling to lower Zeeman levels (both in the doublet and quartet potentials) such that they are not resolved, leading to a lower number of observable resonances. This explains the observed qualitative difference between the upper and lower spin-stretched states.

Finally, we investigate numerically the coupling mechanism that gives rise to the observed resonances. As argued above, each resonance state can essentially be assigned a molecular and a total electron spin quantum number $s_{\mathrm{mol}} = 1$ and $S = 3/2$, as only the nonreactive quartet spin state supports stable resonance states. The resonance is magnetically tunable only if the Zeeman state M_S changes. To couple states with $\Delta M_S \neq 0$ a spin-dependent coupling must be involved through spin-rotation and spin-spin coupling.

From the tensor rank of these couplings we can determine they couple states with the selection rules, $J = 0 \to 1$ and $|\Delta M_S| \leq 1$ (for spin-rotation coupling), and $J = 0 \to 2$ and $|\Delta M_S| \leq 2$ (for spin-spin coupling), respectively. The spin-spin couplings and spin-rotation couplings arise from terms $(\hat{s}_{\mathrm{mol}} \cdot \hat{r})(\hat{s}_{\mathrm{mol}} \cdot \hat{r})$ and $\hat{s}_{\mathrm{mol}} \cdot \hat{N}$ for the NaLi molecule, where $\hat{r}$ points along the molecular axis and $\hat{s}_{\mathrm{mol}}$ is the molecular electronic spin. Since they depend on the orientation of the molecular axis, they cause exchange of spin angular momentum with the molecular rotation N.

Since J is approximately a good quantum number, both mechanisms give rise to distinct and independent resonances. Since the density of states of the collision complex scales with $2J + 1$ and the differential magnetic moment is higher for larger $|\Delta M_S|$ transitions, we conclude that most—approximately $5/6$—of the resonances are due to spin-spin coupling, and the remaining $1/6$ is due to spin-rotation coupling. Spin-spin coupling does not occur for $^2\Sigma$ molecules, and hence is a somewhat unique coupling mechanism for NaLi in the triplet ground state ($^3\Sigma$).

To confirm the role of the spin-dependent interactions in the coupling mechanism, we perform coupled-channels calculations where we reduce these couplings by a factor 2. The resulting cross section multiplied by four is shown as the crosses in Fig. 5(a). The agreement with the full calculation indicates scaling with the square of the coupling

strength that is expected for perturbatively weak spin-dependent couplings. Note that on resonance, the dependence on the coupling strength is not an overall scaling, as the coupling strength also determines the resonance widths. For smaller coupling, the peaks are narrower and higher. Those results confirm that we can fully assign the resonances approximately good quantum numbers $s_{\mathrm{mol}} = 1$, $S = 3/2$, each resonance also has definite M_S constrained by $\Delta M_S \leq 1$ and ≤ 2 selection rules, and $J = 1$ or 2, for spin-rotation and spin-spin coupling, respectively, whereas the N and L quantum numbers are strongly mixed due to the anisotropic interaction at short range. Figure 5(a) also implies that the loss mechanisms are the same for resonant losses and background losses. For the value of λ chosen in Fig. 5(a), the background loss is higher for the upper spin-stretched state, but for most values of λ, they are similar, as observed in the experiment [24].

The coupling mechanism involving the spin-rotation and spin-spin coupling also requires an anisotropic interaction potential. The physical picture is that the anisotropic interaction with the atom can reorient the molecule, and because the spin is coupled to the molecular axis by spin-rotation and spin-spin coupling, this can lead to Zeeman transitions. To confirm this picture we perform calculations that exclude interaction anisotropy, shown as the dash-dotted line in Fig. 5(a). The resulting cross section is much smaller and results from long-range Zeeman relaxation by the magnetic dipole-dipole coupling. If both the magnetic dipole-dipole interaction and the interaction anisotropy are switched off, the cross section in our model vanishes. The role of the interaction anisotropy is nonperturbative, however, as can be seen from comparison between the solid and dotted line in Fig. 5(a), which compares the cross section from the full calculation to 4 times the cross section obtained with the interaction anisotropy halved. The crucial and nonperturbative role of the anisotropic electronic interaction implies that the spectrum of resonances cannot be described by a simplified model that accounts only for the isotropic long-range R^{-6} interaction, contrary to previous observations of ultracold atom-molecule resonances [17]. In summary, the observed losses arise from the interplay of spin-spin and spin-rotation coupling with the anisotropic interactions which connect the incoming nonreactive quartet states to doublet states that can decay to singlet NaLi or Na_2 molecules. This coupling can occur directly, or via first coupling to nonstretched quartet states.

We make a direct comparison to the scattering calculations with the density of states computed quantum mechanically using the same channel basis as used in the scattering calculations in the accompanying paper [24]. The total number of states from the quasiclassical estimate is close to the number of resonances from the scattering calculations, but not in perfect agreement with it, because of the light masses and relatively weak interactions in the spin-stretched state. We find that most of the three-body states are between $20a_0$ and $40a_0$, which is in agreement with the complex size estimated from the simple interpretation of the spacing between resonances as rotational energy splitting of the collision complex. This size is short compared to the range of the van der Waals potential, but much longer than the short-range interactions—the minimum of the potential wells is around $10a_0$. The resonances depend on both short-range and long-range physics: They are supported by the long-range potential, but require the anisotropic short-range interactions as a coupling mechanism.

The calculated widths of the resonances vary between 1 and 30 G, in qualitative agreement with the experiment. Those widths reflect the lifetime since there are no other broadening mechanisms in our simulations. Experimental broadening such as finite resolution of magnetic field strength and magnetic field inhomogeneity is very small (estimated to be around 100 mG near 1400 G).

V. CONCLUSION AND OUTLOOK

We provide a large-scale map of Feshbach resonances between ultracold atoms and molecules. We choose collisions between NaLi in the triplet ground state and Na for the two fully spin-stretched initial collision channels in the quartet potential. Although the NaLi + Na mixture is chemically reactive, there is no reactivity in the quartet potential; i.e., inelastic collisions require a spin flip to the doublet potential [18,19]. The possibility of metastable collision complexes makes this system promising for the study of Feshbach resonances. Indeed, we observe 8 and 17 resonances within a ∼1400 G range in the upper and lower stretched states, respectively.

We compare the experimental results to full coupled-channel calculations for the NaLi + Na mixture. Even state-of-the-art quantum-chemistry calculations cannot predict the position of resonances because of the uncertainty in the interaction potentials. However, they can provide a deep understanding of the relevant states and their couplings. Our simulations show that the resonance states are three-body complexes in the quartet state with rotational excitation, either of NaLi (quantum number N) or rotation of Na around NaLi (quantum number L). These complexes have a typical size of $30a_0$–$40a_0$. The input state and the complex state involve different M_S, which is necessary for a magnetic Feshbach resonance. Molecular eigenstates in different Zeeman levels can be coupled by a strong anisotropic electronic interaction since the different molecular Zeeman states have different rotational state decompositions mainly due to spin-spin coupling and also spin-rotation coupling. Note that the spin-rotation and spin-spin coupling depend on the orientation of the molecular axis and, therefore, provide tensorial couplings between the spin and the mechanical angular momentum. Approximately 5/6 of the resonances can be attributed to spin-spin coupling to states with total mechanical angular

momentum $J = 2$, and the remaining $1/6$ is attributed to spin-rotation coupling and assigned $J = 1$.

The loss of molecules, either the background loss or via Feshbach resonances, occurs through transition to the chemically reactive doublet potential, either directly or through lower Zeeman states of the quartet potential (for the upper stretched state). These transitions involve an interplay of the anisotropic electronic interaction with spin-spin or spin-rotation coupling in the NaLi molecules. Dipolar transitions are considerably weaker.

Our coupled-channels calculations explain why the number of observed resonances is smaller for the upper stretched state. The upper stretched state supports a similar number of resonances, but several of them are washed out by the rapid decay of the intermediate complexes to lower-lying Zeeman states via spin-spin coupling.

The agreement between experiment and calculations validates the assumptions made in the calculations. At least for a semiquantitative analysis, it is sufficient to neglect hyperfine interactions and vibrationally excited states of the molecules, and use electronic potentials at fixed nuclear separation for the molecule.

The physical mechanisms we identify in the Na + NaLi($a^3\Sigma^+$) mixture are unique to molecules in the triplet or higher-spin state. It would be interesting to study other bialkali triplet molecules and check if their collision dynamics is dominated by similar couplings. The only other case where atom-molecule Feshbach resonances have been studied involved NaK in the singlet ground state [16,17]. For this system, the observed Feshbach resonances were caused by long-range van der Waals interactions [17,30]. These long-range states then follow regular patterns dictated by the quantum defect theory for a simple isotropic long-range R^{-6} interaction [31]. The resonances we describe here, however, behave quite differently as the coupling mechanism involves perturbatively the spin-spin and spin-rotation coupling and the strong nonperturbative anisotropic interaction at short range. Although the resulting resonances are supported by the long-range interaction, their positions are sensitive to these anisotropic short-range interactions and hence cannot be described by the regular patterns predicted by quantum defect theory.

Our work here focuses on the nonreactive quartet potential to support metastable collisional complexes. However, recent studies have shown that collisional resonances and collisional complexes should also occur in highly reactive systems. A single p-wave Feshbach resonance has been observed in collisions between NaLi molecules in the triplet ground state [21]. This system has no barrier for reactions. Losses much smaller than the universal loss rate have been observed in s-wave collisions between magnetically trapped NaLi molecules in different hyperfine states of the triplet state [32], a system which should be highly reactive. Losses far below the universal rate imply a nonzero reflection probability at short range and should lead to Feshbach resonances when the magnetic field tuning creates strong interference between reflections at short and long range [18,33].

These studies emphasize that our understanding of reactivity and metastable collisional complexes is incomplete, and further experimental explorations are required. Further studies should involve NaLi in various hyperfine states and with various collision partners, as well as considering other bialkalis. As suggested in Ref. [30], for nonstretched states, the Fermi contact interaction between electron and nuclear spin provides another mechanism for Feshbach resonances. Such broader studies are required to find out which mechanisms are universal, and which occur only in specific systems.

ACKNOWLEDGMENTS

The MIT work was supported by the NSF through the Center for Ultracold Atoms and Grant No. 1506369 and by the Air Force Office of Scientific Research (MURI, Grant 613 No. FA9550-21-1-0069). J. J. P. and H. S. acknowledge additional support from the Samsung Scholarship. M. G. and M. T. were supported by the National Science Centre Poland (Sonata Bis Grant No. 2020/38/E/ST2/00564) and the PL-Grid Infrastructure (Computational Grant No. PLG/2020/014342).

APPENDIX: STATISTICAL ANALYSIS

A statistical analysis of the separations between resonances can provide insight into the nature of the resonant states. We quantify the resonance statistics of 17 resonances from Na + NaLi collisions in the lower stretched state provided in Table I using the Brody parameter η, which is a standard measure of chaos. For nonchaotic systems, in which resonances have no correlations, the distribution of nearest-neighbor spacings is given by the Poisson distribution, $P_P(s) = e^{-s}$. On the other hand, for chaotic systems, which emerge when the mean spacing between bound states is comparable to the coupling strength, repulsion between energy levels occurs. In this regime, the distribution of nearest-neighbor spacings is given by a Wigner-Dyson distribution, $P_{\mathrm{WD}}(s) = (\pi/2)se^{-(\pi/4)s^2}$ [25,26]. The two distributions are smoothly interpolated through the Brody parameter η as $P_B(s) = As^\eta e^{-[A/(\eta+1)]\cdot s^{\eta+1}}$, known as the Brody distribution, where $A = (\eta+1)\cdot\Gamma(\eta+2/\eta+1)^{\eta+1}$ [34,35]. Here, $\eta = 1$ and $\eta = 0$ lead to the Wigner-Dyson and Poisson distributions, respectively. The cumulative probability function of the Brody distribution is given as

$$F_B(s) = (\eta+1)\cdot[1 - e^{-\alpha s^{\eta+1}}]. \tag{A1}$$

Figure 6 shows the cumulative probability of resonance spacing of the 17 resonances from Na + NaLi collisions in the lower stretched state. The best fit of the data to Eq. (A1)

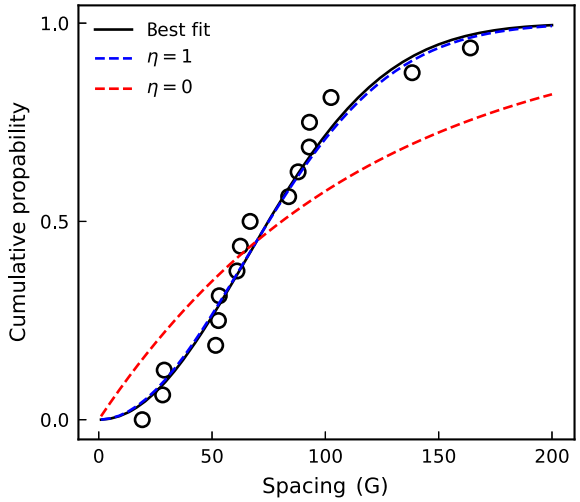

FIG. 6. Cumulative probability of resonance spacings. Shown are the experimental results for Na + NaLi collisions in the lower stretched state. Black line is the best fit to the cumulative probability function of the Brody distribution [Eq. (A1)] and the blue (red) dashed line is the cumulative distribution with $\eta = 1$ ($\eta = 0$).

gives $\eta = 1.1(1)$, which shows the statistical signature of quantum chaos.

However, statistical conclusions from only 17 resonances are tentative. On the basis of our quantum-scattering calculations, the Wigner-Dyson statistics is not expected because each resonance can be assigned by M_S, J, and M_J quantum numbers (resonances with different values for these quantum numbers do not affect each other). In addition, it is difficult to conclude that the broad trend of the distribution of resonance widths follows the Porter-Thomas distribution of resonance widths, $P_{\mathrm{PT}}(\bar{\gamma}) = \bar{\gamma}^{-1/2} e^{-\bar{\gamma}/2}$, which is also a statistical character of quantum chaos. Here, the scaled reduced widths $\bar{\gamma} = \gamma_n^0 / \langle \gamma_n^0 \rangle$, where γ_n^0 is the resonance width normalized by the resonance energy, and $\langle \gamma_n^0 \rangle$ is the average of γ_n^0 [36]. Figure 7 shows the histogram of the scaled reduced resonance width distribution and the Porter-Thomas distribution. Because of the small statistical sample, it is difficult to compare the broad trend of the distribution with the Porter-Thomas distribution. Nevertheless, Fig. 6 represents a purely empirical analysis of experimental data, which should find a theoretical explanation (which is probably not quantum chaos).

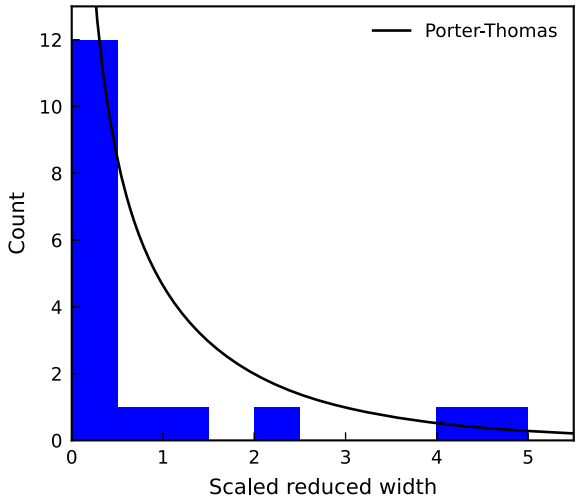

FIG. 7. Distribution of scaled reduced widths for scattering resonances. This plot is based on the data for the lower stretched state Na + NaLi mixture listed in Table I. The black line shows the Porter-Thomas distribution of scaled reduced widths.

[1] C. Chin, R. Grimm, P. Julienne, and E. Tiesinga, *Feshbach Resonances in Ultracold Gases*, Rev. Mod. Phys. **82**, 1225 (2010).

[2] I. Bloch, J. Dalibard, and S. Nascimbene, *Quantum Simulations with Ultracold Quantum Gases*, Nat. Phys. **8**, 267 (2012).

[3] B. Zhao and J.-W. Pan, *Quantum Control of Reactions and Collisions at Ultralow Temperatures*, Chem. Soc. Rev. **51**, 1685 (2022).

[4] M. Mayle, B. P. Ruzic, and J. L. Bohn, *Statistical Aspects of Ultracold Resonant Scattering*, Phys. Rev. A **85**, 062712 (2012).

[5] A. Christianen, T. Karman, and G. C. Groenenboom, *Quasiclassical Method for Calculating the Density of States of Ultracold Collision Complexes*, Phys. Rev. A **100**, 032708 (2019).

[6] M. Morita and T. V. Tscherbul, *Restricted Basis Set Coupled-Channel Calculations on Atom-Molecule Collisions in Magnetic Fields*, J. Chem. Phys. **150**, 074110 (2019).

[7] S. Koyu, R. Hermsmeier, and T. V. Tscherbul, *Total Angular Momentum Representation for State-to-State Quantum Scattering of Cold Molecules in a Magnetic Field*, J. Chem. Phys. **156**, 034112 (2022).

[8] A. O. Wallis, E. J. Longdon, P. S. Żuchowski, and J. M. Hutson, *The Prospects of Sympathetic Cooling of NH Molecules With Li Atoms*, Eur. Phys. J. D **65**, 151 (2011).

[9] M. Morita, R. V. Krems, and T. V. Tscherbul, *Universal Probability Distributions of Scattering Observables in Ultracold Molecular Collisions*, Phys. Rev. Lett. **123**, 013401 (2019).

[10] M. Mayle, G. Quéméner, B. P. Ruzic, and J. L. Bohn, *Scattering of Ultracold Molecules in the Highly Resonant Regime*, Phys. Rev. A **87**, 012709 (2013).

[11] A. Christianen, G. C. Groenenboom, and T. Karman, *Lossy Quantum Defect Theory of Ultracold Molecular Collisions*, Phys. Rev. A **104**, 043327 (2021).

[12] C. Chin, T. Kraemer, M. Mark, J. Herbig, P. Waldburger, H.-C. Nägerl, and R. Grimm, *Observation of Feshbach-like Resonances in Collisions between Ultracold Molecules*, Phys. Rev. Lett. **94**, 123201 (2005).

[13] S. Knoop, F. Ferlaino, M. Mark, M. Berninger, H. Schöbel, H.-C. Nägerl, and R. Grimm, *Observation of an Efimov-like*

Trimer Resonance in Ultracold Atom-Dimer Scattering, Nat. Phys. **5**, 227 (2009).

[14] A. Zenesini, B. Huang, M. Berninger, H.-C. Nägerl, F. Ferlaino, and R. Grimm, *Resonant Atom-Dimer Collisions in Cesium: Testing Universality at Positive Scattering Lengths*, Phys. Rev. A **90**, 022704 (2014).

[15] F. Wang, X. Ye, M. Guo, D. Blume, and D. Wang, *Observation of Resonant Scattering between Ultracold Heteronuclear Feshbach Molecules*, Phys. Rev. A **100**, 042706 (2019).

[16] H. Yang, D.-C. Zhang, L. Liu, Y.-X. Liu, J. Nan, B. Zhao, and J.-W. Pan, *Observation of Magnetically Tunable Feshbach Resonances in Ultracold* ^{23}Na^{40}K + ^{40}K *Collisions*, Science **363**, 261 (2019).

[17] X.-Y. Wang, M. D. Frye, Z. Su, J. Cao, L. Liu, D.-C. Zhang, H. Yang, J. M. Hutson, B. Zhao, C.-L. Bai *et al.*, *Magnetic Feshbach Resonances in Collisions of* ^{23}Na^{40}K *with* ^{40}K, New J. Phys. **23**, 115010 (2021).

[18] H. Son, J. J. Park, Y.-K. Lu, A. O. Jamison, T. Karman, and W. Ketterle, *Control of Reactive Collisions by Quantum Interference*, Science **375**, 1006 (2022).

[19] M. Tomza, K. W. Madison, R. Moszynski, and R. V. Krems, *Chemical Reactions of Ultracold Alkali-Metal Dimers in the Lowest-Energy* $^3\Sigma$ *State*, Phys. Rev. A **88**, 050701(R) (2013).

[20] H. Son, J. J. Park, W. Ketterle, and A. O. Jamison, *Collisional Cooling of Ultracold Molecules*, Nature (London) **580**, 197 (2020).

[21] J. J. Park, Y.-K. Lu, A. O. Jamison, T. V. Tscherbul, and W. Ketterle, *A Feshbach Resonance in Collisions between Triplet Ground-State Molecules*, Nature (London) **614**, 54 (2023).

[22] R. Hermsmeier, J. Kłos, S. Kotochigova, and T. V. Tscherbul, *Quantum Spin State Selectivity and Magnetic Tuning of Ultracold Chemical Reactions of Triplet Alkali-Metal Dimers with Alkali-Metal Atoms*, Phys. Rev. Lett. **127**, 103402 (2021).

[23] T. M. Rvachov, H. Son, A. T. Sommer, S. Ebadi, J. J. Park, M. W. Zwierlein, W. Ketterle, and A. O. Jamison, *Long-Lived Ultracold Molecules with Electric and Magnetic Dipole Moments*, Phys. Rev. Lett. **119**, 143001 (2017).

[24] T. Karman, M. Gronowski, M. Tomza, J. J. Park, H. Son, Y.-K. Lu, A. O. Jamison, and W. Ketterle, companion paper, *Ab Initio Calculation of the Spectrum of Feshbach Resonances in* NaLi + Na *Collisions*, Phys. Rev. A **108**, 023309 (2023).

[25] E. P. Wigner, *On a Class of Analytic Functions from the Quantum Theory of Collisions*, in *The Collected Works of Eugene Paul Wigner* (Springer, Berlin, Heidelberg, 1993), pp. 409–440, 10.1007/978-3-662-02781-3_26.

[26] F. J. Dyson, *Statistical Theory of the Energy Levels of Complex Systems. I*, J. Math. Phys. **3**, 140 (1962).

[27] S. Knoop, T. Schuster, R. Scelle, A. Trautmann, J. Appmeier, M. K. Oberthaler, E. Tiesinga, and E. Tiemann, *Feshbach Spectroscopy and Analysis of the Interaction Potentials of Ultracold Sodium*, Phys. Rev. A **83**, 042704 (2011).

[28] M. Steinke, H. Knöckel, and E. Tiemann, $(X)1^1\Sigma^+$ *State of LiNa Studied by Fourier-Transform Spectroscopy*, Phys. Rev. A **85**, 042720 (2012).

[29] T. M. Rvachov, H. Son, J. J. Park, S. Ebadi, M. W. Zwierlein, W. Ketterle, and A. O. Jamison, *Two-Photon Spectroscopy of the NaLi Triplet Ground State*, Phys. Chem. Chem. Phys. **20**, 4739 (2018).

[30] M. D. Frye and J. M. Hutson, *Complexes Formed in Collisions between Ultracold Alkali-Metal Diatomic Molecules and Atoms*, New J. Phys. **23**, 125008 (2021).

[31] M. D. Frye and J. M. Hutson, *Long-Range States and Feshbach Resonances in Collisions between Ultracold Alkali-Metal Diatomic Molecules and Atoms*, Phys. Rev. Res. **5**, 023001 (2023).

[32] J. J. Park, Y.-K. Lu, A. O. Jamison, and W. Ketterle, *Magnetic Trapping of Ultracold Molecules at High Density*, arXiv:2211.11120.

[33] P. S. Julienne, T. M. Hanna, and Z. Idziaszek, *Universal Ultracold Collision Rates for Polar Molecules of Two Alkali-Metal Atoms*, Phys. Chem. Chem. Phys. **13**, 19114 (2011).

[34] T. Brody, *A Statistical Measure for the Repulsion of Energy Levels*, Lett. Nuovo Cimento **7**, 482 (1973).

[35] T. A. Brody, J. Flores, J. B. French, P. Mello, A. Pandey, and S. S. Wong, *Random-Matrix Physics: Spectrum and Strength Fluctuations*, Rev. Mod. Phys. **53**, 385 (1981).

[36] C. E. Porter and R. G. Thomas, *Fluctuations of Nuclear Reaction Widths*, Phys. Rev. **104**, 483 (1956).